Earthquake Induced Damage Mitigation from Soil Liquefaction

CLASS A PREDICTION FOR LIQUEFACTION REMEDIATION INITIATIVE CENTRIFUGE TEST 7(LRICT7)

By:
Ahmad Jafari

Supervisor: Dr. Radu Popescu

Memorial University of Newfoundland
February, 2005

Introduction

In this report Class A prediction of the 7th LRI (Liquefaction Remediation Initiative) centrifuge test (LRICT7) is presented.

LRICT7 geometry and input motion

General layout and target input motion for class A prediction of LRICT7 are similar to those of LRICT6. The only difference between LRICT7 and LRICT6 is the existence of an inclined silt layer in LRICT7 with a slope of 1:5.7. The location of the silt layer is the same as LRICT5, but there are no drainage dykes in LRICT7. The input acceleration time history used in this test is A2475 with a magnification factor of 2, i.e. 2×A2475. Like LRICT5 and LRICT6, the FE model for this prediction consists of 588 nodes and 542 elements.

Soil properties

Results of centrifuge tests COSTA-C2 and LRICT5 with silt layer have indicated softer behavior in the centrifuge tests compared to their corresponding numerical predictions. This may be related to two reasons; first, there was no relevant information regarding the silt layer and the set of silt parameters used in class A prediction of LRICT5 was only based on judgment and experience. Another reason is believed to be related to the way that sand slopes are prepared in the centrifuge model. To obtain a smooth face of the slope, the sand is shaped with the aid of vacuum. This is believed to loosen the sand in a narrow layer immediately below the slope face. Loosening of a small amount of sand at the ground surface is believed not to affect the general slope behavior, and it was not considered for the predictions of models up to LRICT6 (including LRICT5, which had a silt layer). In tests LRICT7 and 8 besides the sand face at the ground surface, the sand immediately below the inclined silt layer is also processed with vacuum. Since presence of very loose sand immediately below the silt layer may be important for the general behavior of the model, it was decided to include a narrow layer of sand (about 1.5 cm at the model scale) at about 20% relative density. Soil properties considered for this narrow sand layer below the silt are listed in Table 1. The dilation parameter of this looser sand

is estimated from numerical simulation of the results of isotropically consolidated cyclic triaxial tests performed on Fraser River sand samples by Dr. Vaid. Estimation of the value of hydraulic conductivity for the narrow looser sand by extrapolating the corresponding value of this parameter at a relative density of 40% to get a value at 20% results in about 20% increase in the value of hydraulic conductivity. This increase is neglected in this prediction.

Previous centrifuge tests results showed that the silt layer and the soil mass above it had a rigid block type movement. Therefore, the silt is believed to be stronger than initially estimated for class A prediction of LRICT5. Also, the silt permeability is considered to be 1/1000 of that of the sand. The new silt parameters and parameters considered for the narrow sand layer below the silt, are listed in Table 1.

Constitutive parameters	**Symbol**	**Assumed values**	
		Silt	**Looser sand**
Mass density (kg/m^3) Porosity Hydraulic conductivity (permeability) (cm/s)	ρ_s n^w k	2670 0.448 0.0000084	2710 0.467 0.0084
Low-strain shear modulus (Mpa) Reference effective mean normal stress Powe exponent Poisson ratio	G_0 p_0 n ν	5 100 0.8 0.4	15 100 0.5 0.3
Friction angle at failure Coefficient of lateral earth pressure at rest Soil cohesion Maximum deviatoric strain (C= compression, E=extension)	ϕ k_0 c ε^{max}_{dev}	25^o 1 0 0.06 (C), 0.06 (E)	35^o 1 0 0.02 (C), 0.01 (E)
Dilation angle (phase transformation angle) Dilation parameter	Ψ X_{PP}	17^o 0.01	34^o 0.55

Table 1 Assumed constitutive parameters for silt and looser sand layers

(Looser sand: Only for two rows of elements immediately below the silt of about 1.2 m)

Results of Class A prediction of LRICT7

Results of class A prediction of LIRCT7 are shown in Figures 1 to 23 at prototype scale as predicted displacements, excess pore pressure ratios, and accelerations for all transducer positions. For 10 s < t < 20 s, the numerical model predicts significant dilation (large negative excess pore water pressure) at EPP4, EPP8, and Epp9, which are located at shallow depths. The predicted contours of maximum shear strain at the end of analysis (t=42.54 s) are shown in Figure 24 along with the deformed shape of the model. Figures 25 to 29 show contours of excess pore water pressure ratios at different instants. As it can be seen from these figures, the excess pore water pressures below the silt layer increase after the end of earthquake, i.e. after about t=20 s.

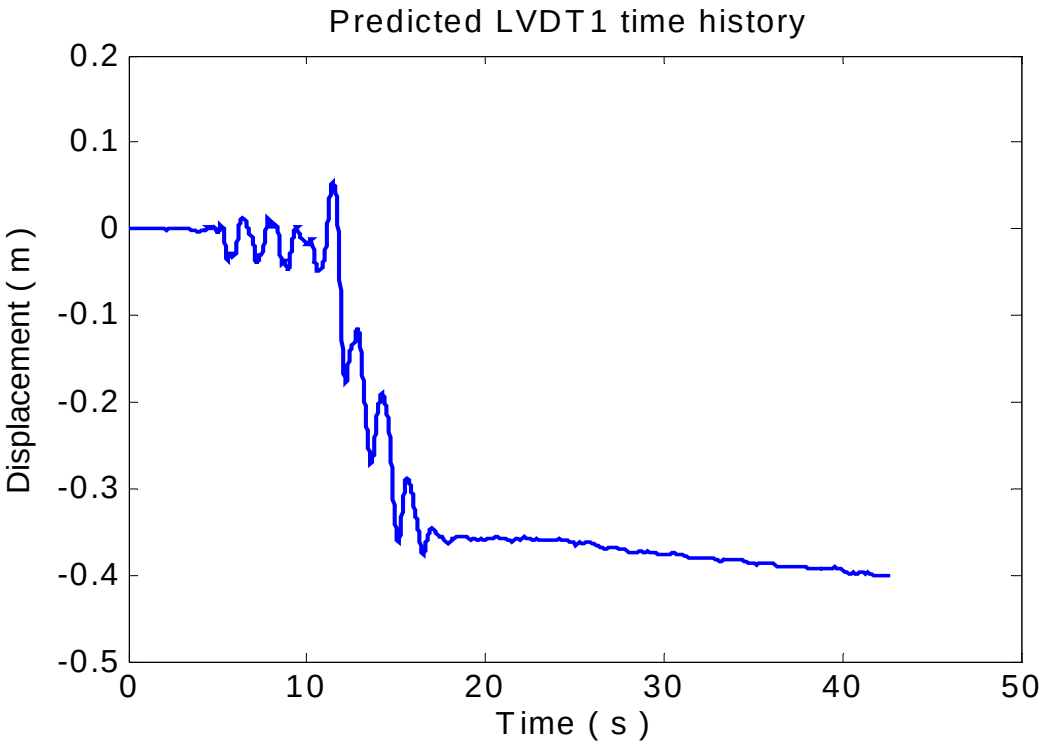

Fig. 1 Predicted LVDT1 time history

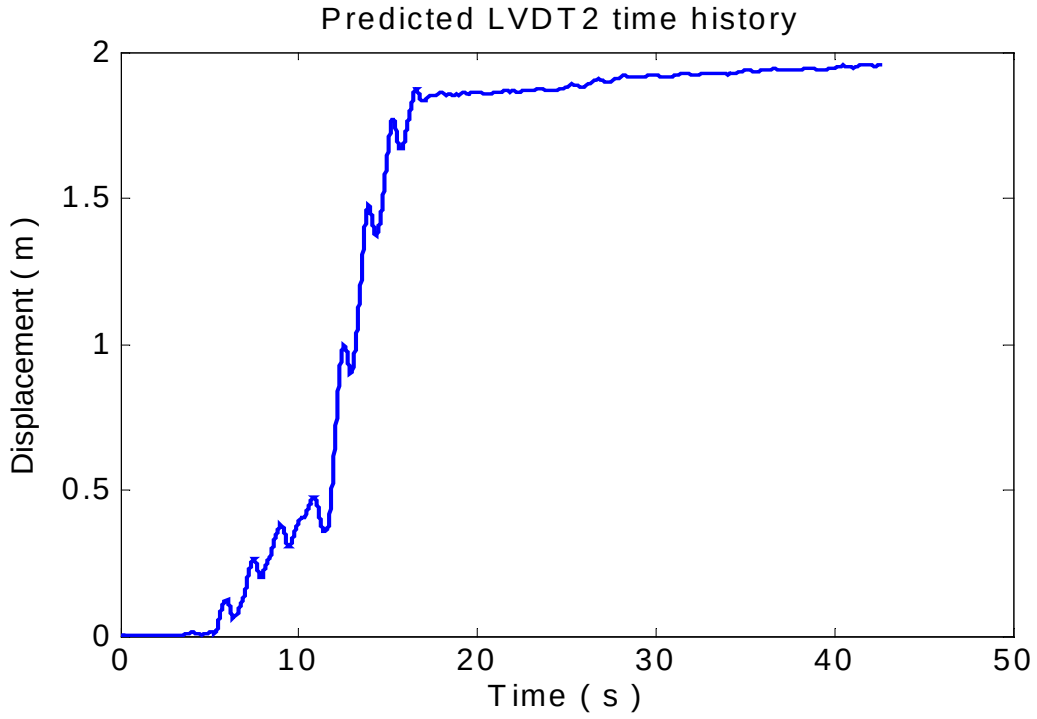

Fig. 2 Predicted LVDT2 time history

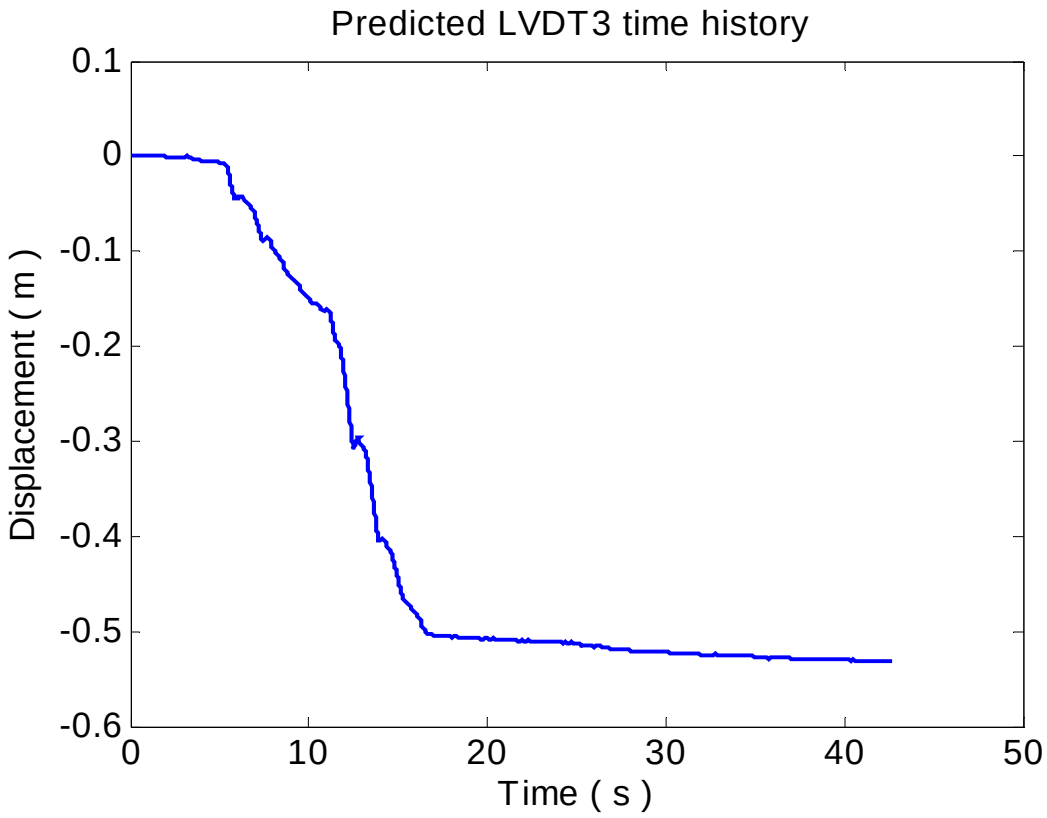

Fig. 3 Predicted LVDT3 time history

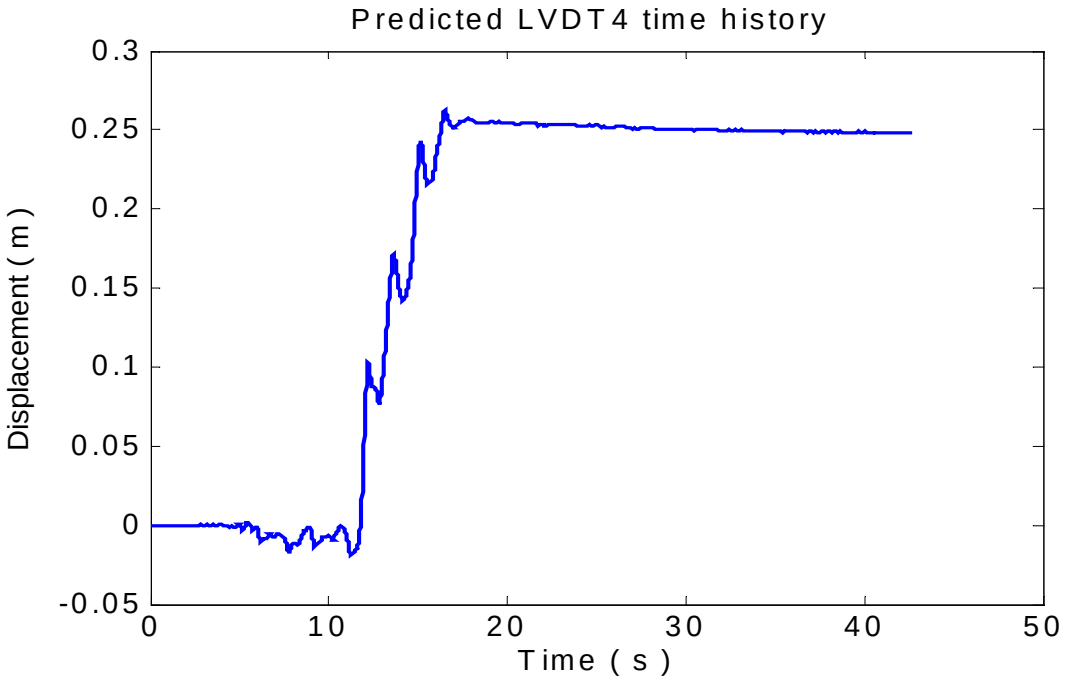

Fig. 4 Predicted LVDT4 time history

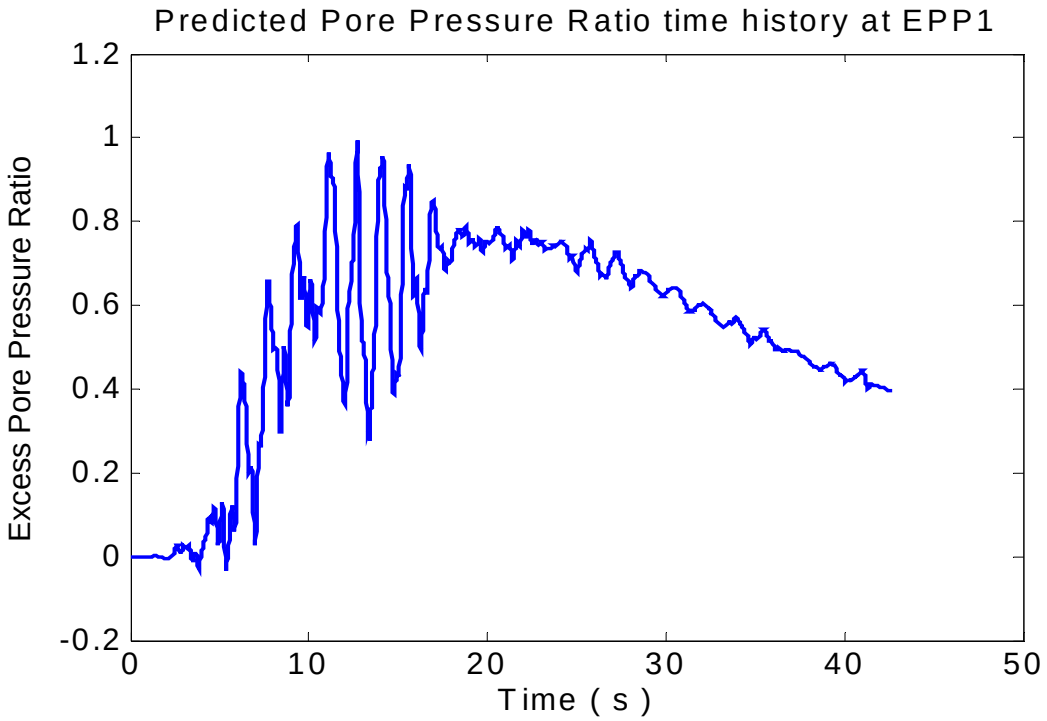

Fig. 5 Predicted EPP1 time history (IVES=122 KPa)

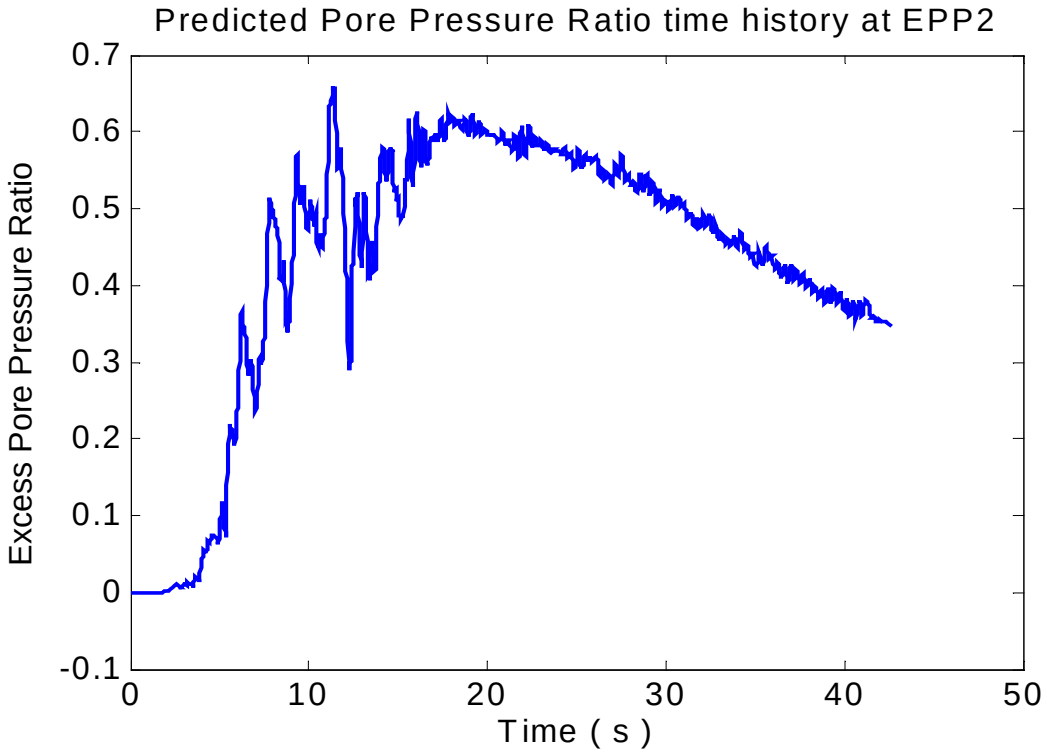

Fig. 6 Predicted EPP2 time history (IVES=120 KPa)

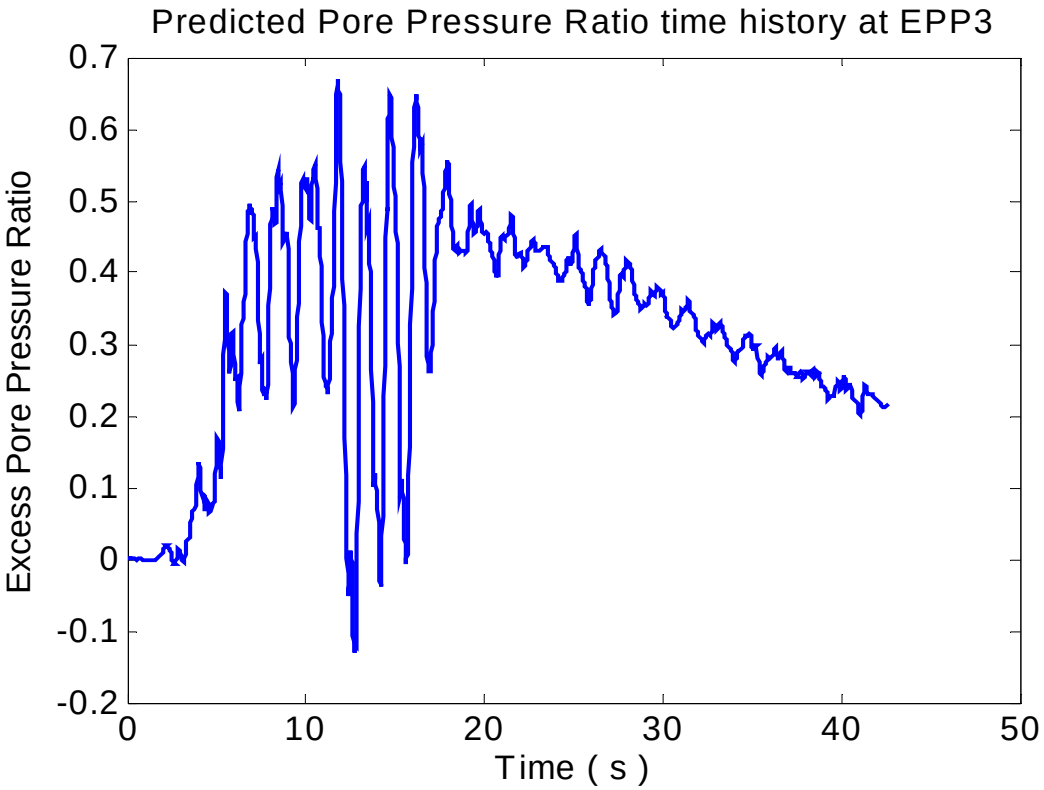

Fig. 7 Predicted EPP3 time history (IVES=88 KPa)

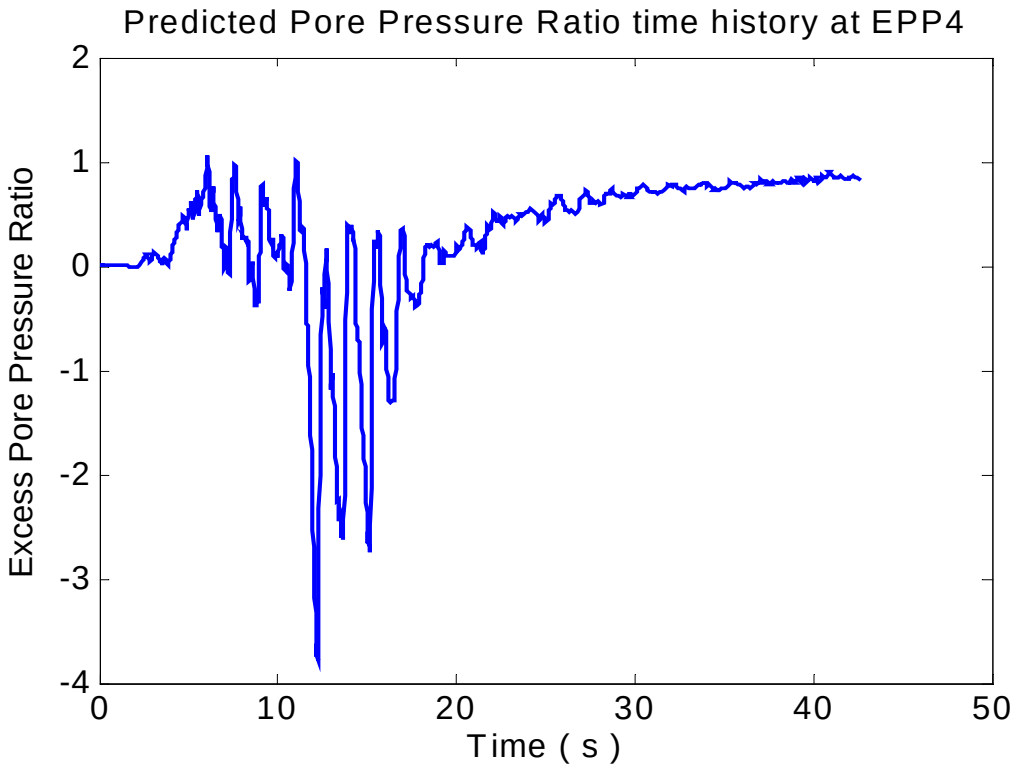

Fig. 8 Predicted EPP4 time history (IVES=12 KPa)

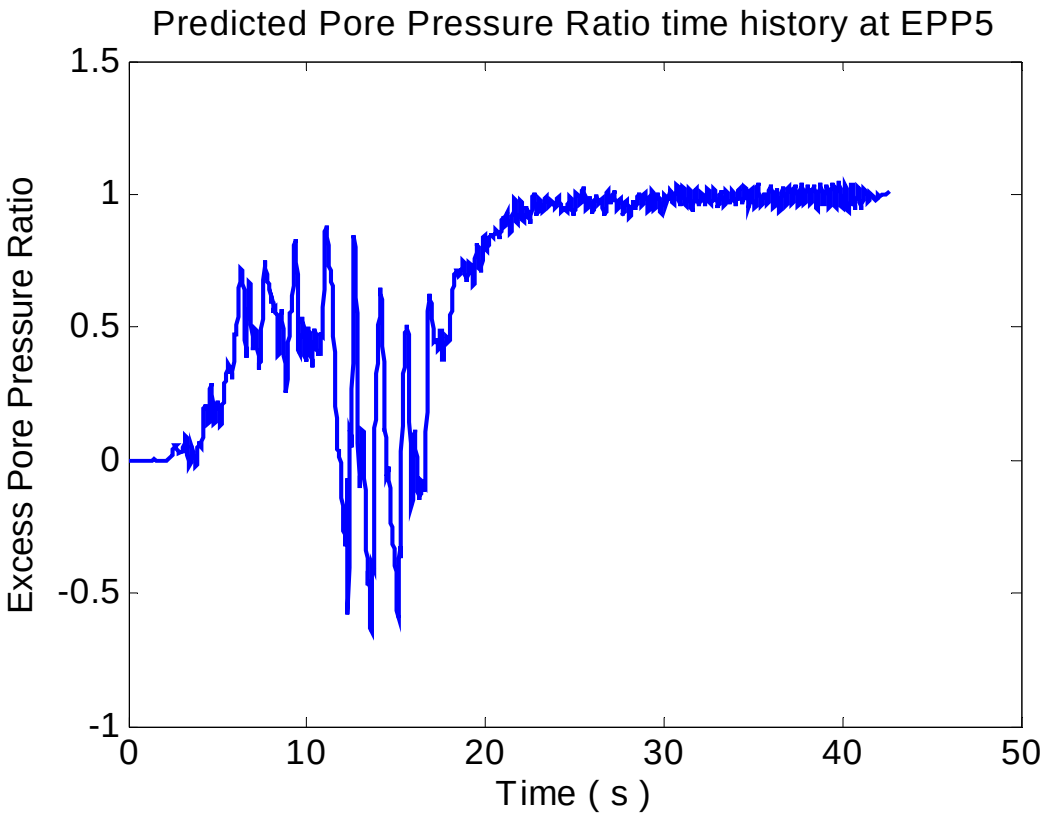

Fig. 9 Predicted EPP5 time history (IVES=25 KPa)

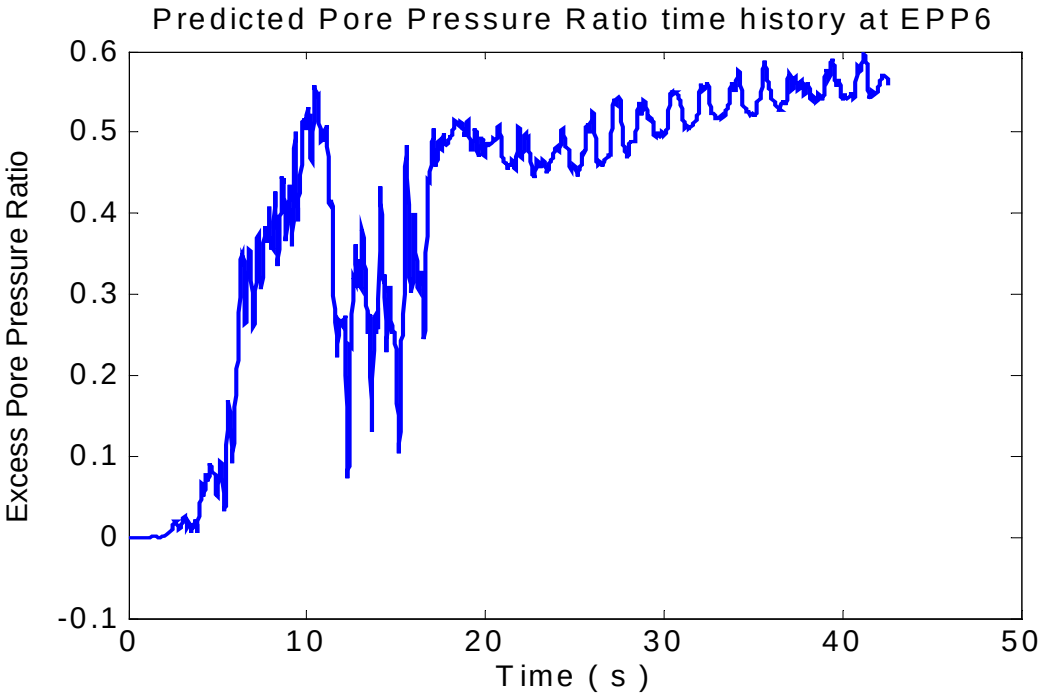

Fig. 10 Predicted EPP6 time history (IVES=58 KPa)

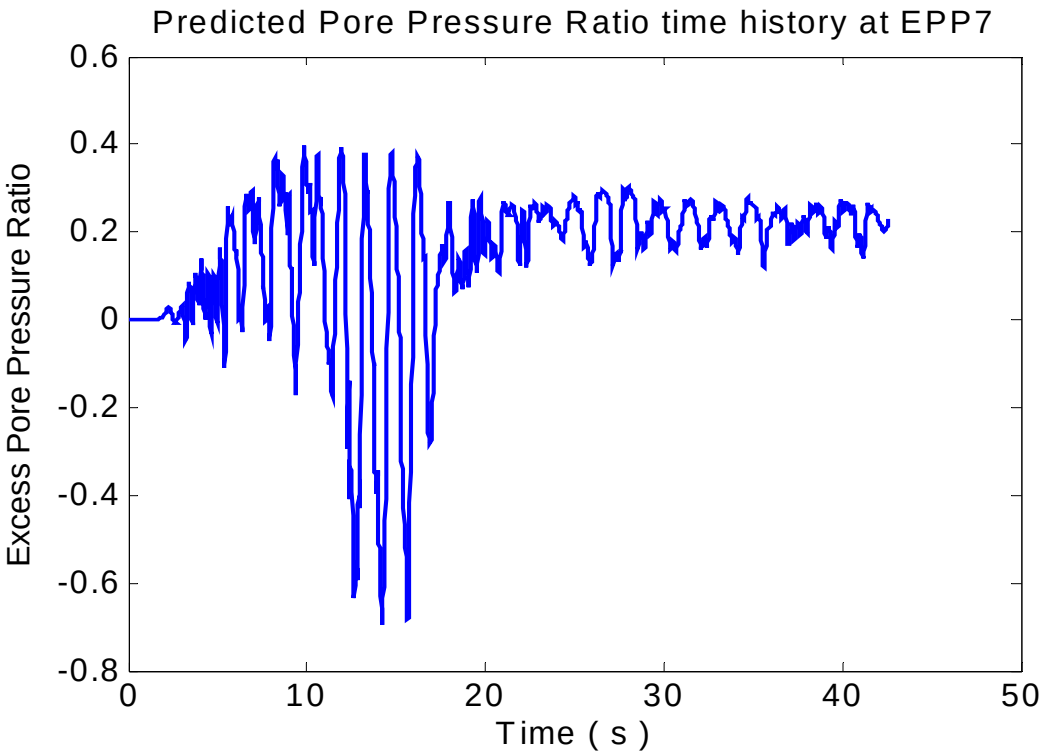

Fig. 11 Predicted EPP7 time history (IVES=34 KPa)

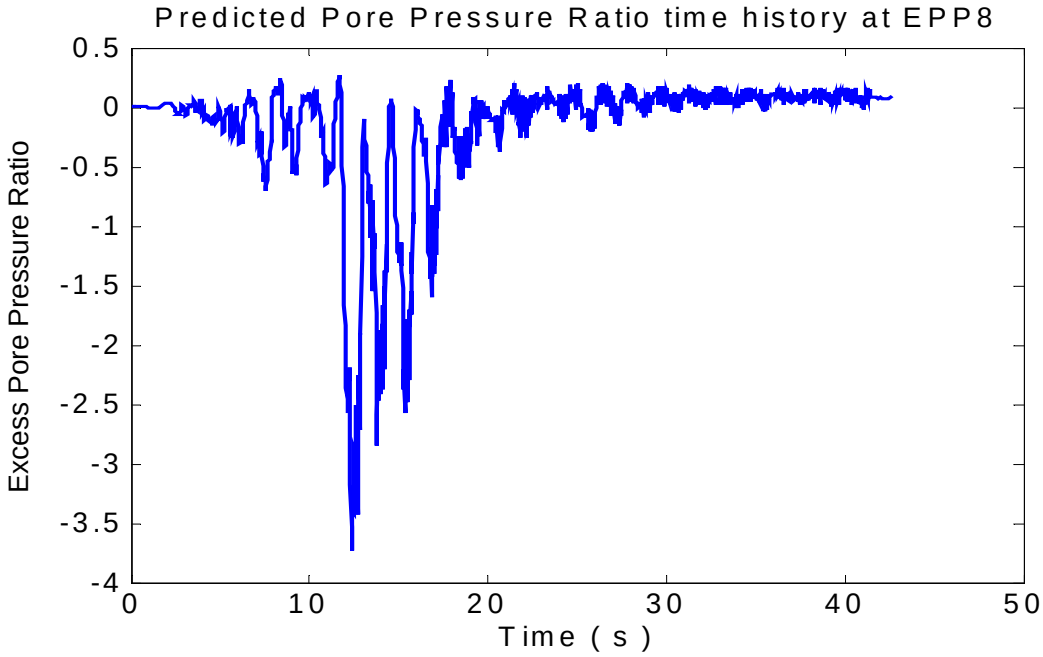

Fig. 12 Predicted EPP8 time history (IVES=14 KPa)

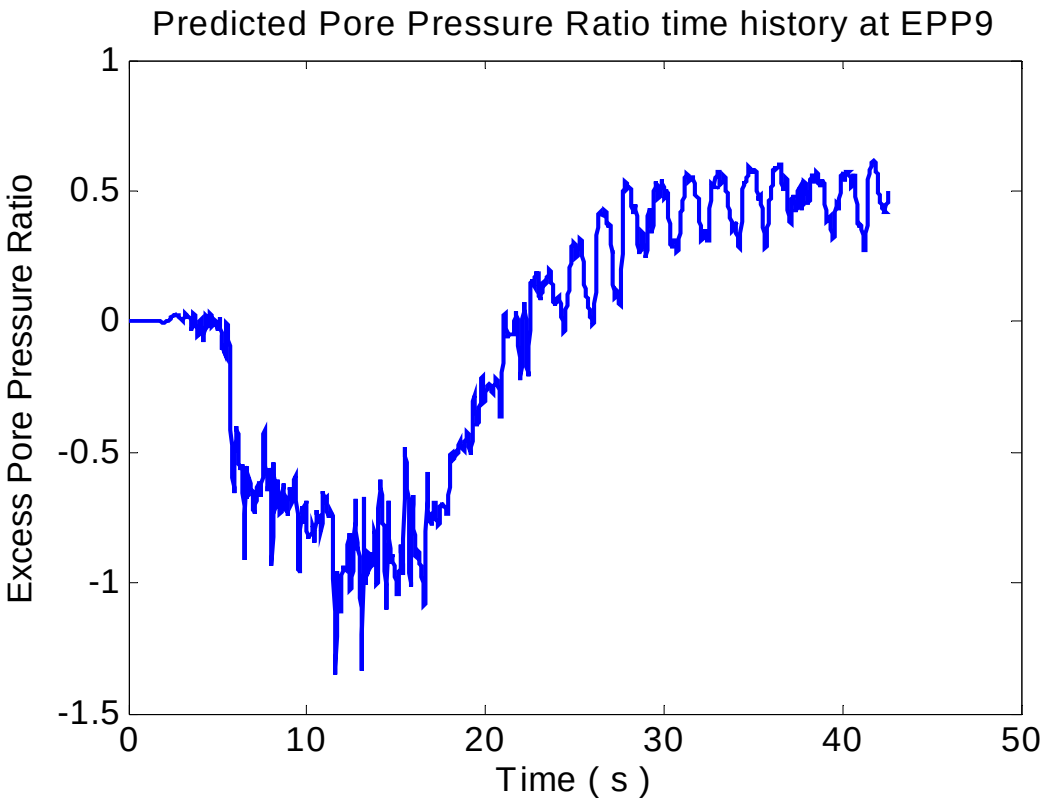

Fig. 13 Predicted EPP9 time history (IVES=14 KPa)

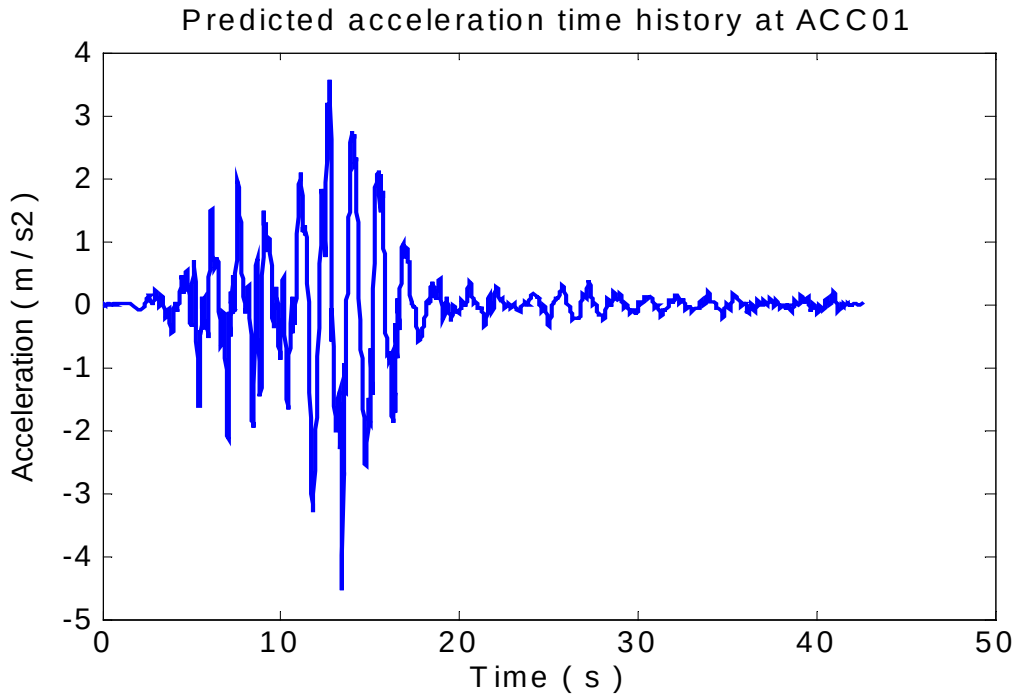

Fig. 14 Predicted acceleration time history at ACC01

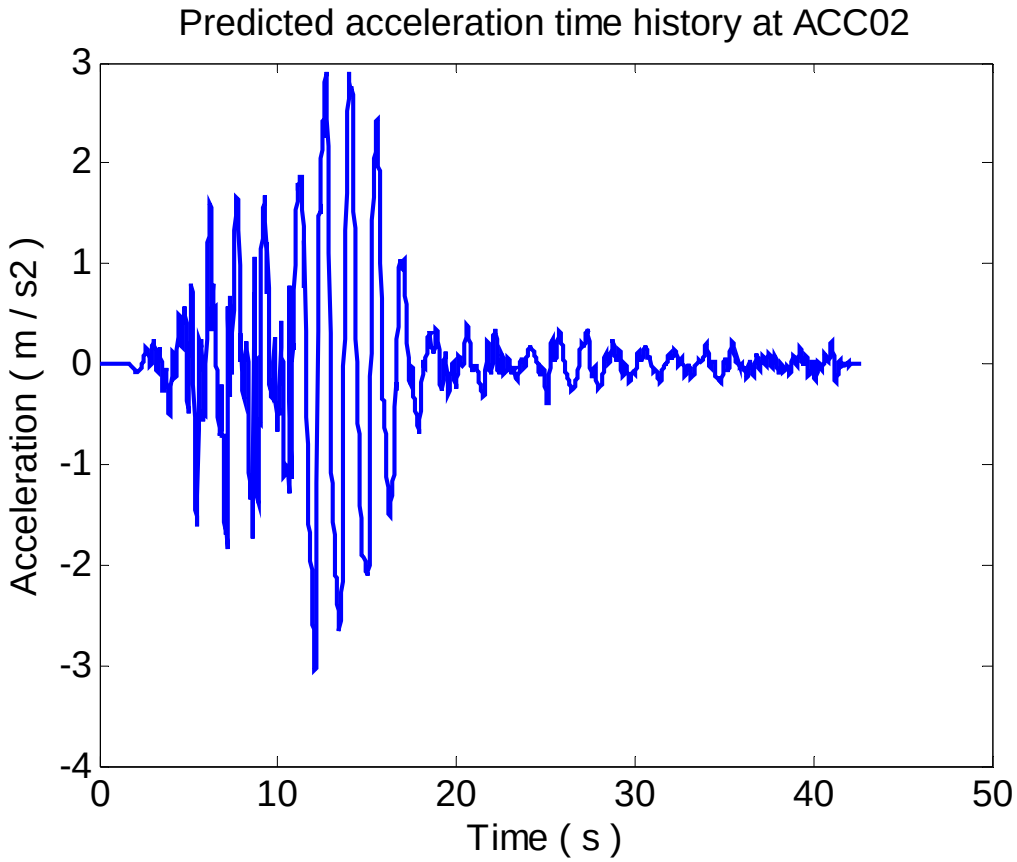

Fig. 15 Predicted acceleration time history at ACC02

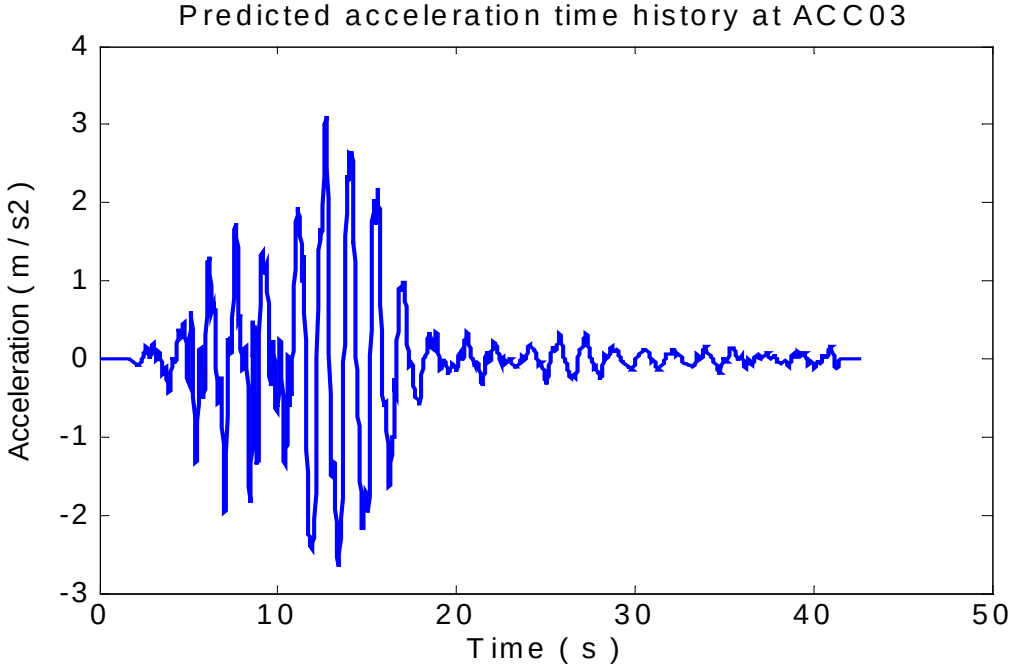

Fig. 16 Predicted acceleration time history at ACC03

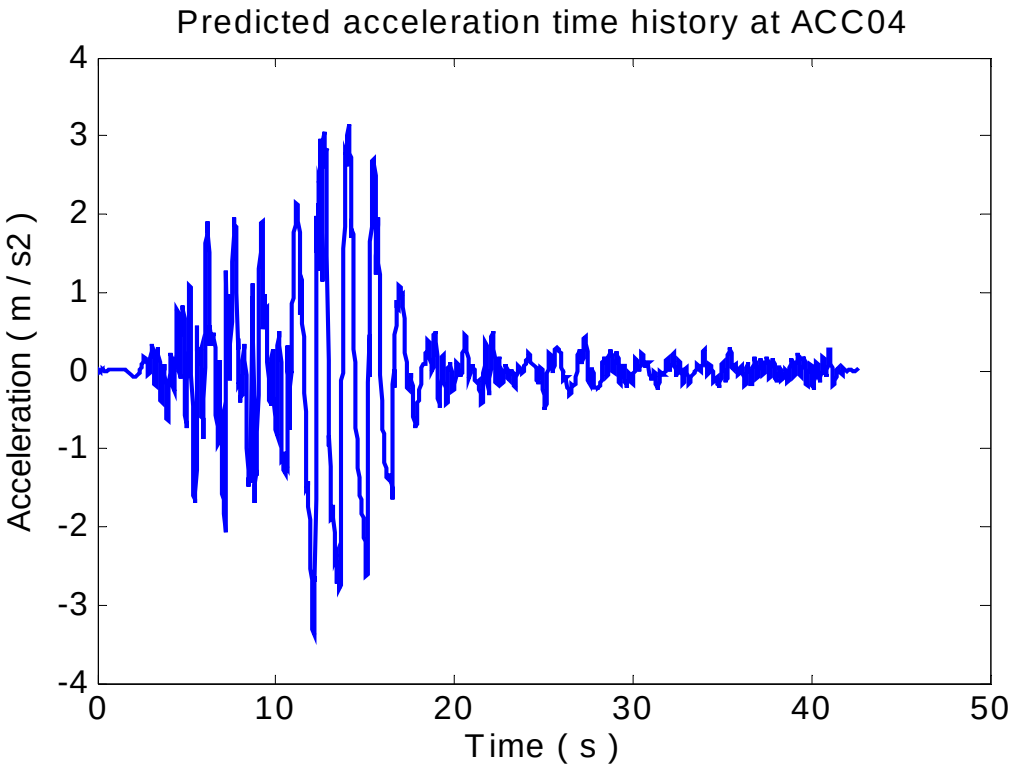

Fig. 17 Predicted acceleration time history at ACC04

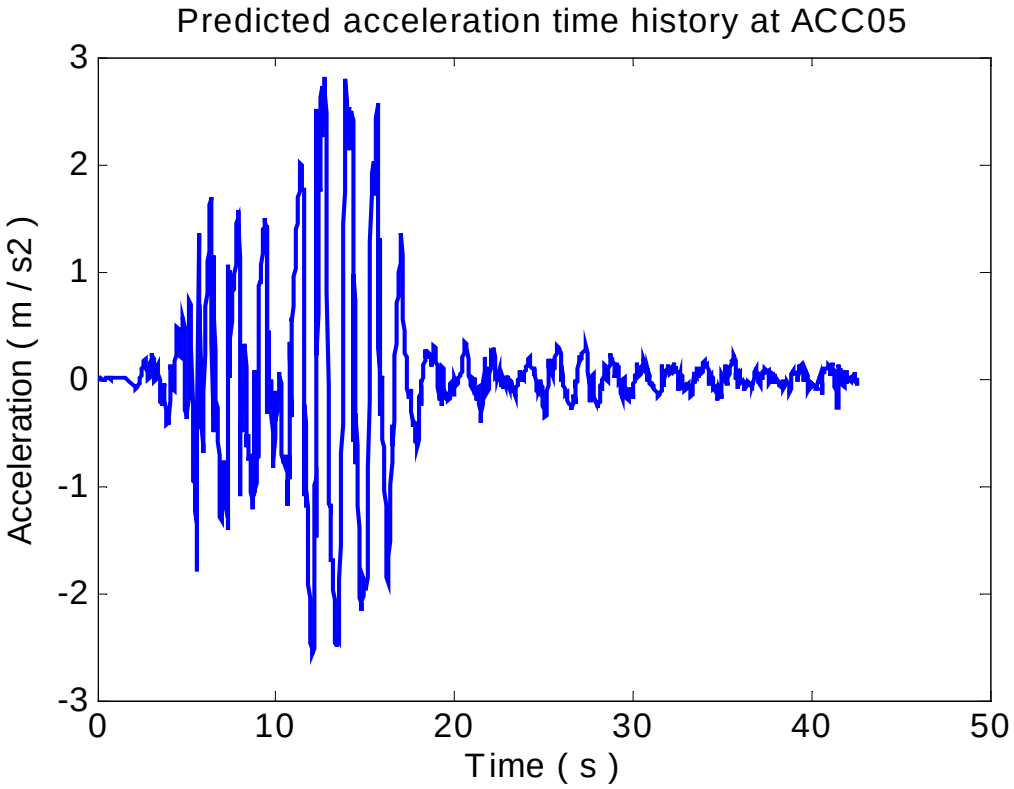

Fig. 18 Predicted acceleration time history at ACC05

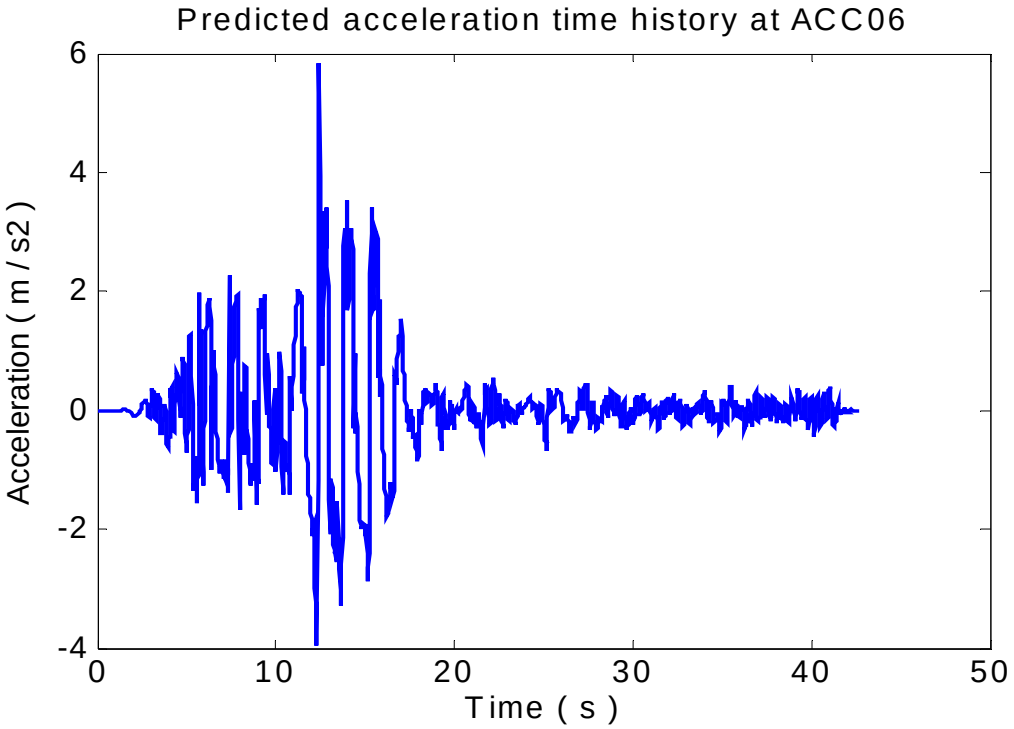

Fig. 19 Predicted acceleration time history at ACC06

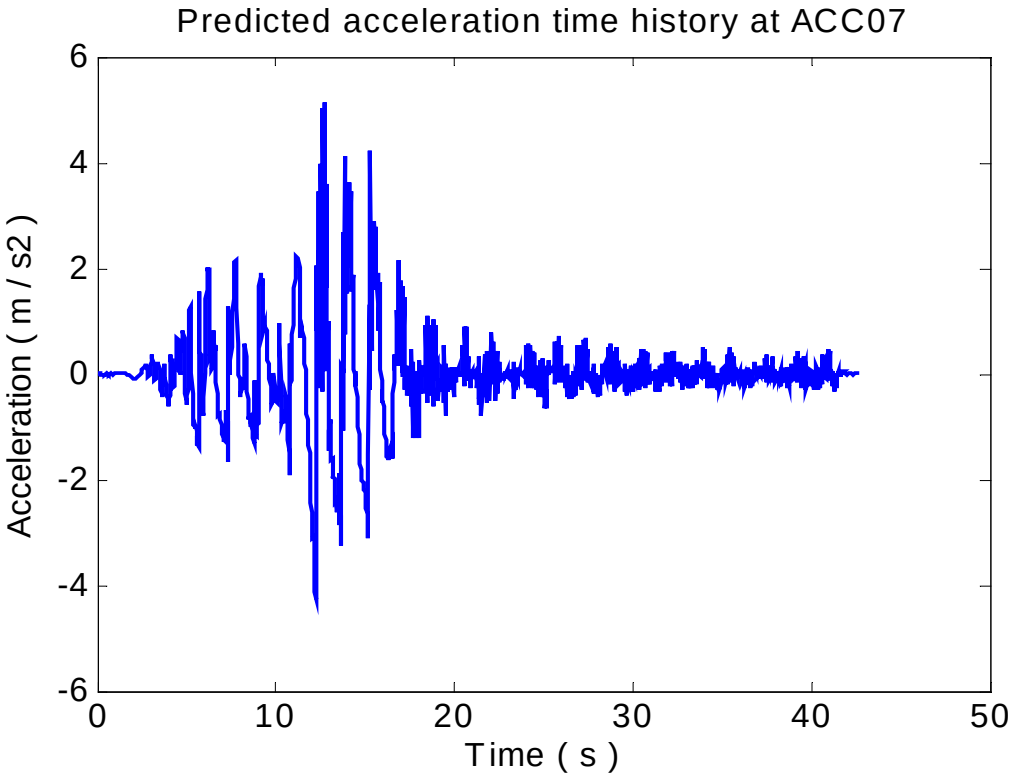

Fig. 20 Predicted acceleration time history at ACC07

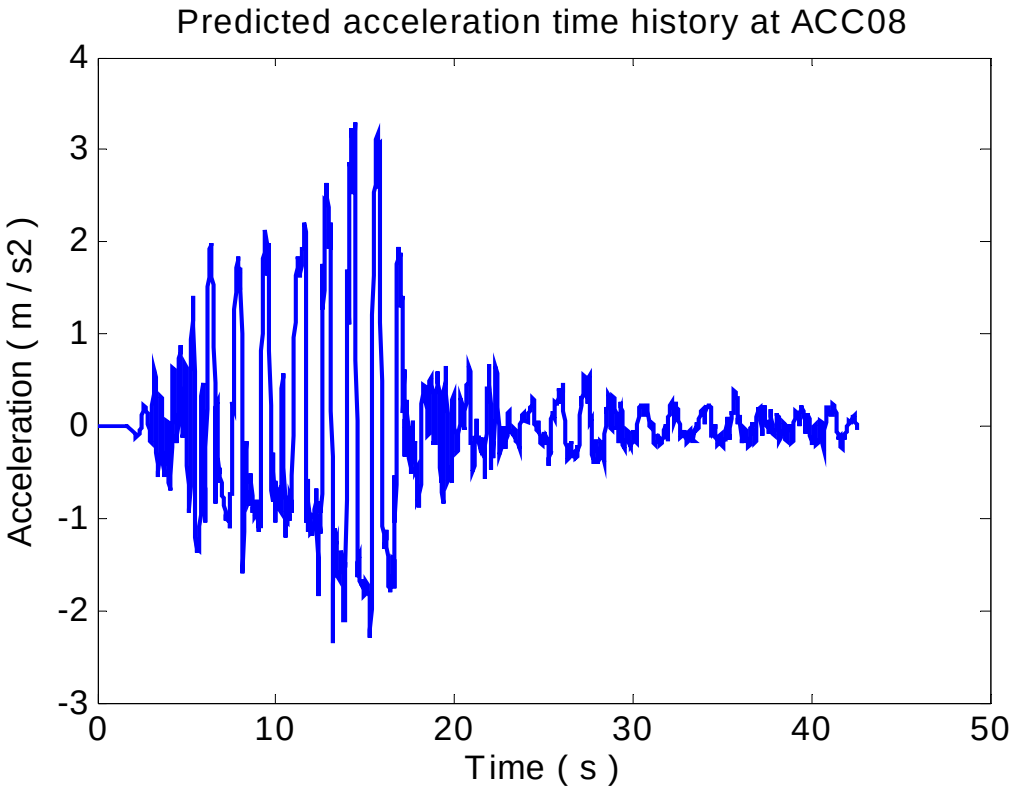

Fig. 21 Predicted acceleration time history at ACC08

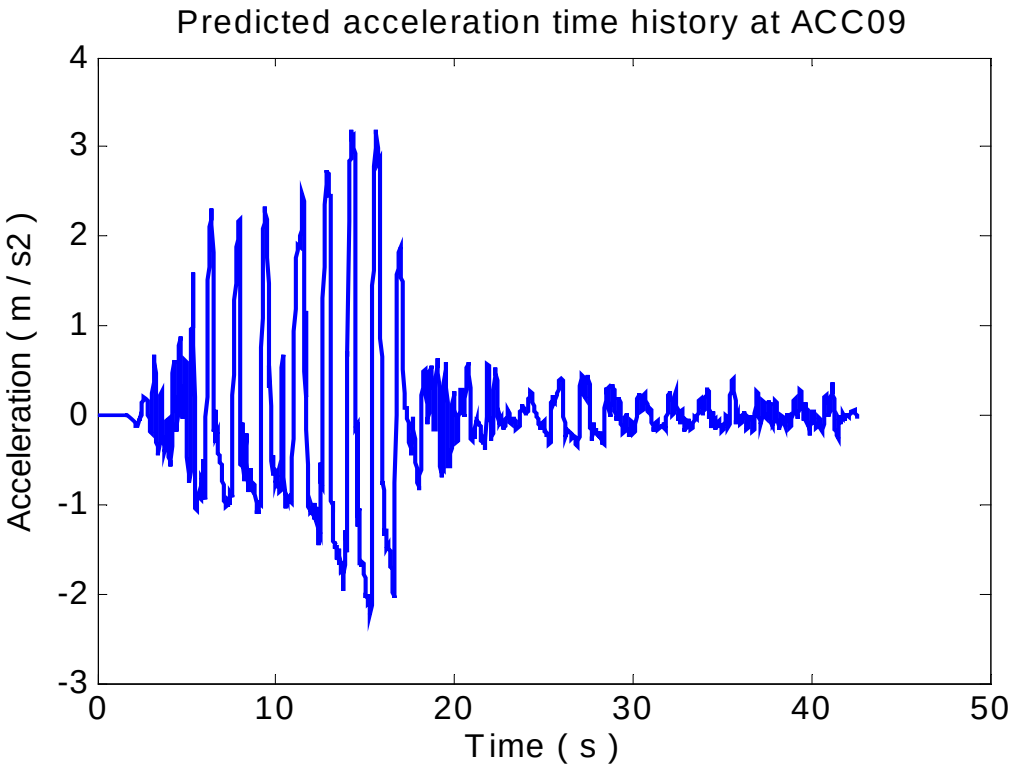

Fig. 22 Predicted acceleration time history at ACC09

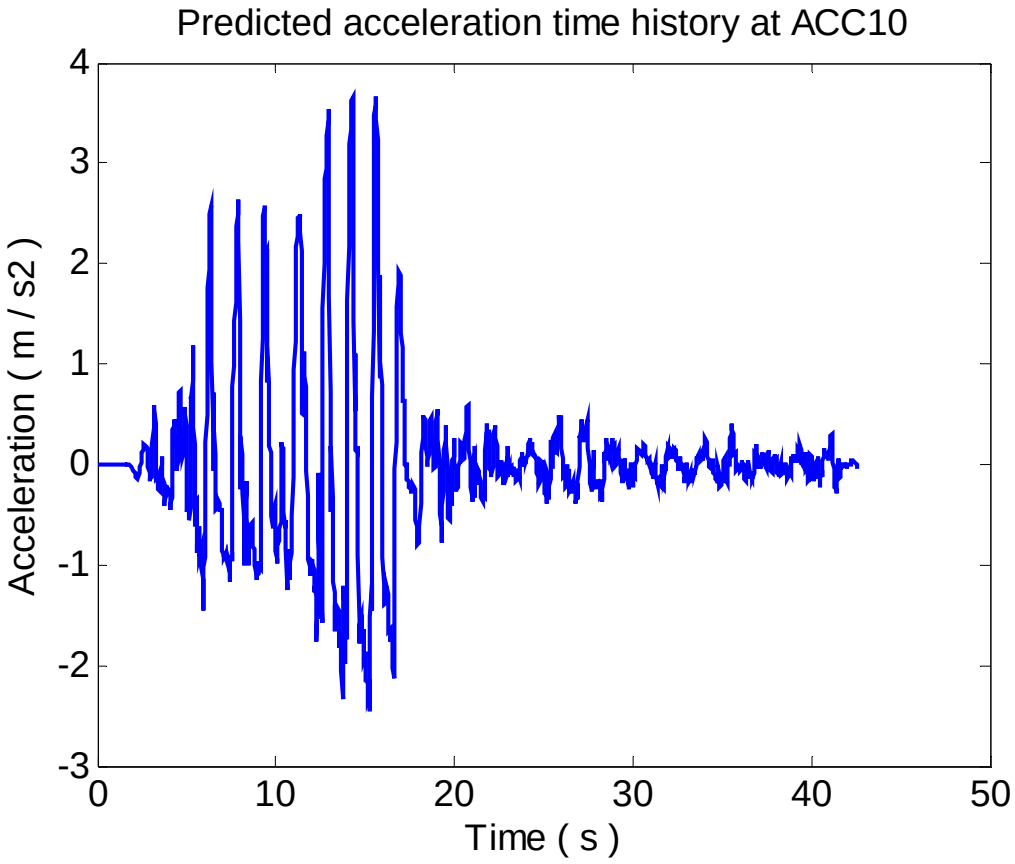

Fig. 23 Predicted acceleration time history at ACC10

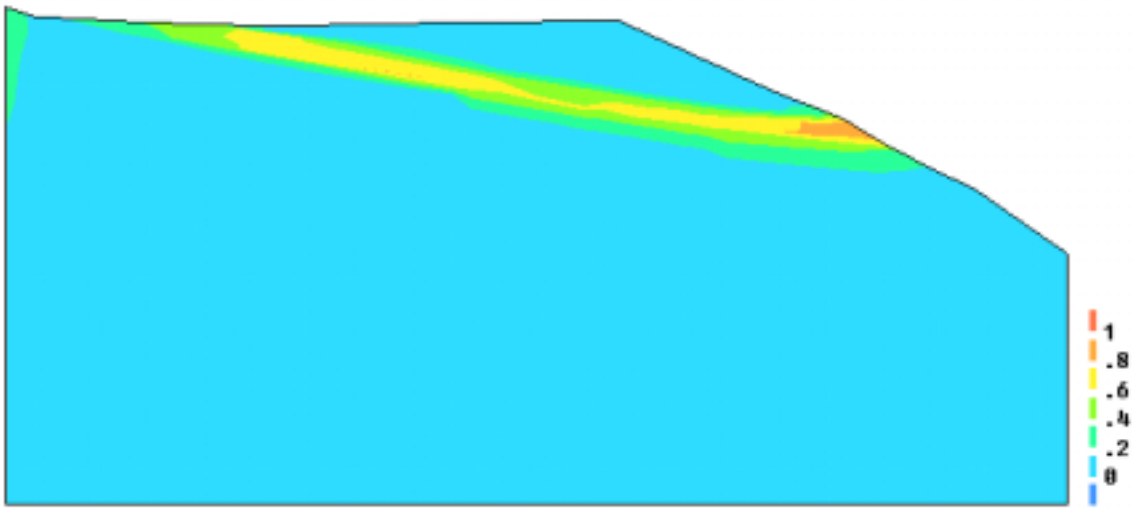

Fig. 24 Predicted maximum shear strain contours at the end of analysis, t=42.54 s (Deformed shape magnification factor=1)

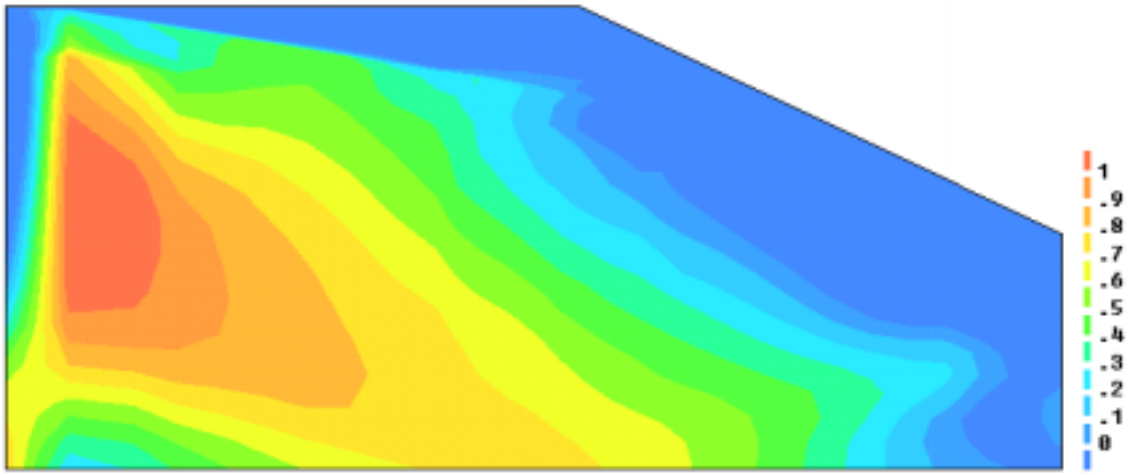

Fig. 25 Predicted contours of excess pore water pressure ratio at t=14 s

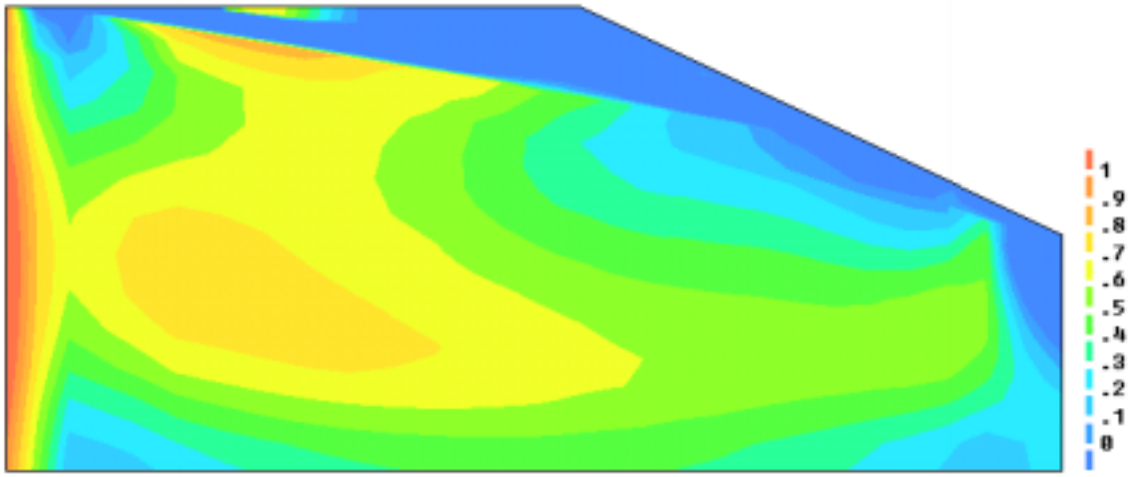

Fig. 26 Predicted contours of excess pore water pressure ratio at t=20 s

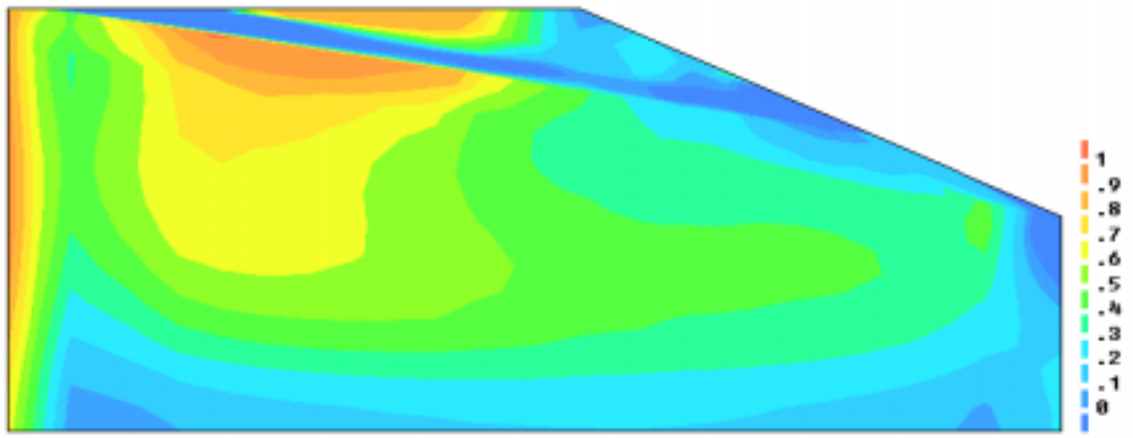

Fig. 27 Predicted contours of excess pore water pressure ratio at t=28 s

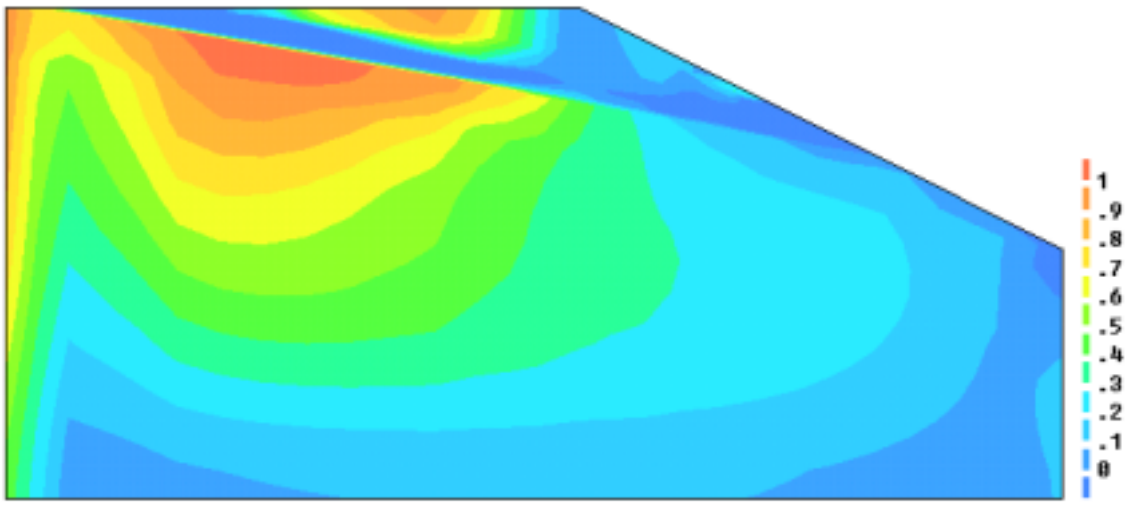

Fig. 28 Predicted contours of excess pore water pressure ratio at t=36 s

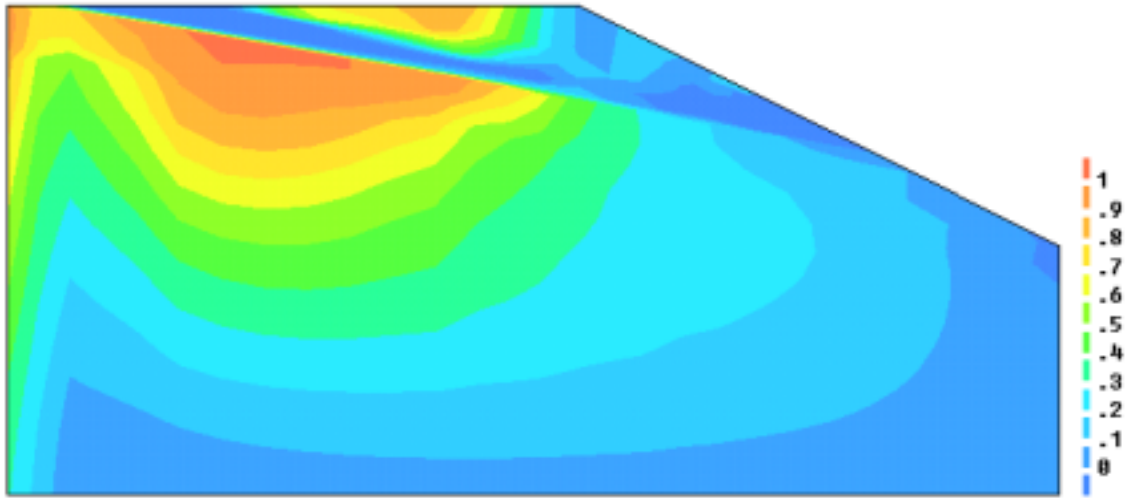

Fig. 29 Predicted contours of excess pore water pressure ratio at end of analysis, t=42.54s